17

Dawn-Dusk Asymmetries of Solar-Wind–Magnetosphere Coupling in the Earth's Midtail

Chih-Ping Wang[1], Xiaoyan Xing[2], T. K. M. Nakamura[3], Larry R. Lyons[4], and Vassilis Angelopoulos[5]

ABSTRACT

Solar-wind–magnetosphere coupling causes plasma exchange across the magnetopause. Using ARTEMIS observations, we investigated dawn-dusk asymmetries and responsible coupling processes for two distinct populations in the midtail ($r \sim 60\ R_E$): (1) mantle plasma resulting from magnetosheath plasma coming through the open magnetopause and (2) bursty hot electron enhancements (HEEs) in the magnetosheath resulting from magnetosphere electrons coming out with transient magnetopause deformation. Mantle plasma appears more frequently in the postmidnight (premidnight) sector above the current sheet when the IMF B_y is positive (negative). Good agreement between the observations and global MHD simulations indicates that the dawn-dusk asymmetry is caused by the open magnetopause moving to the opposite sides of the magnetosphere above and below the current sheet as the IMF B_y becomes more dominant. The HEE occurrence rates are two to three times higher on the dawn side. HEEs correlate more strongly than magnetosheath plasma with sharper transient changes in IMF direction and magnetosheath density and with quasiparallel bow shock. These correlations suggest that perturbations created at the quasiparallel bow shock can possibly cause magnetopause deformation and HEEs in the midtail, contributing to the HEE asymmetry because the quasiparallel bow shock is more often on the dawn side.

17.1. INTRODUCTION

Solar-wind–magnetosphere coupling leads to transfer of plasma, momentum, and energy across the magnetopause, the essential process that drives the dynamics of the Earth's magnetosphere. Two distinct plasma populations resulting from the coupling are: (1) magnetosheath-like mantle plasma observed in the magnetosphere flowing tailward along the open magnetic field lines but with lower density and tailward speed than in the magnetosheath and (2) energetic magnetosphere ions and electrons observed in the magnetosheath. These two populations are associated with different coupling processes, but both populations exhibit clear dawn-dusk asymmetries in their appearance indicting asymmetries in the responsible processes.

For mantle plasma formation, solar-wind plasma entry through the magnetopause along open field lines has been suggested to be an important process [*Siscoe and Sanchez*, 1987; *Siscoe et al.*, 2001]. While the polar ionosphere outflow can also be a source for mantle plasma, studies using Geotail observations of different ion species [e.g., *Seki et al.*, 2000] conclude that most of protons in the mantle have come from the solar wind. The appearance of mantle plasma has been observed in the near-Earth

[1] *Department of Atmospheric and Oceanic Sciences, University of California, Los Angeles, California, USA*

[2] *XS Research LLC, Irvine, California, USA*

[3] *Space Research Institute, Austrian Academy of Sciences, Graz, Austria*

[4] *Department of Atmospheric and Oceanic Sciences, University of California, Los Angeles, California, USA*

[5] *Department of Earth, Planetary, and Space Sciences, University of California, Los Angeles, California, USA*

Dawn-Dusk Asymmetries in Planetary Plasma Environments, Geophysical Monograph 230, First Edition.
Edited by Stein Haaland, Andrei Runov, and Colin Forsyth.

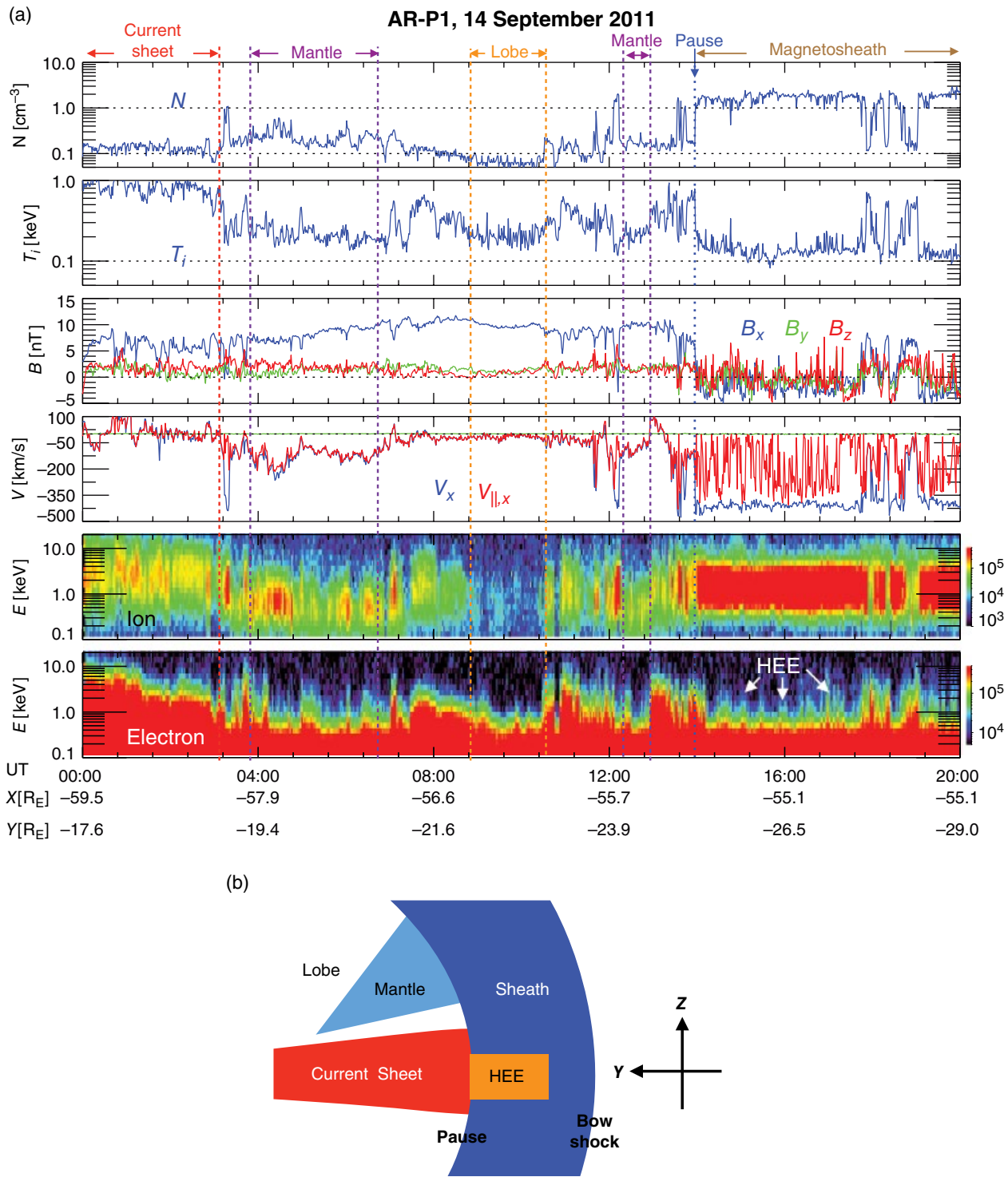

Figure 17.1 (a) An example of ARTEMIS crossing of the midtail magnetosphere and magnetosheath. The magnetopause crossing is indicated by the gray vertical arrow. The intervals of the mantle, the lobe, and the magnetosheath are indicated on the top of the figure enclosed by the vertical dotted lines and horizontal arrows. HEE indicates hot electron enhancements and the white arrows indicate a few examples of HEEs. (b) A simple sketch of the different plasma regimes identified in (a).

region [e.g., *Haerendel and Paschmann*; 1975; *Taguchi et al.*, 2001], at lunar distances [e.g., *Hardy et al.*, 1975, 1976, 1979], and in the distant tail [e.g., *Gosling et al.*, 1984; *Maezawa and Hori*, 1998; *Seki et al.*, 1998]. These observations have shown that its appearance on the dawn or dusk side is strongly correlated with the IMF B_y direction.

On the other hand, energetic particles observed in the magnetosheath can result from energetic magnetosphere particles having access to the magnetosheath either through leakage due to their large gyroradius [*Sibeck et al.*, 1987] or through interconnected magnetosphere-magnetosheath magnetic field lines [*Scholer et al.*, 1981]. Enhancement of energetic electrons with energies from ~15 keV up to hundreds of keV have been observed in the near-Earth magnetosheath. The previous observations have noted a dawn-dusk asymmetry in the enhancements of energetic electrons (>~38 keV) in the near-Earth magnetosheath [e.g., *Sarafopoulos et al.*, 2000; *Imada et al.*, 2005], but not in low-energy (~3 keV) electrons [*Imada et al.*, 2005]. This asymmetry is suggested to be caused by magnetosphere electron fluxes being higher on the dawn side than on the dusk side.

Since late 2010, ARTEMIS has provided observations of mantle plasma and energetic particle enhancement in the magnetosheath in the midtail ($-70 < X < -30$ R_E). The abundant ARTEMIS data also allow for determining the dawn-dusk asymmetries of these two populations with statistical significance. Figure 17.1a shows an example of an ARTEMIS crossing of the midtail from the magnetosphere to the magnetosheath. In the magnetosphere, mantle plasma can be identified as cold (a few hundred eV) plasma with substantial tailward field-aligned speed. Mantle plasma can be seen to appear at low latitudes adjacent to the current sheet where plasma is hotter (a few keV for ions). Within the magnetosheath, ARTEMIS sometimes observed bursty (several minutes) enhancements of hot (~1–10 keV) electrons, called hot electron enhancements (HEEs). These different plasma regimes are sketched in Figure 17.1b. Using ARTEMIS two-point measurements, *Wang et al.* [2014b] concluded that the hot electrons in HEEs are magnetosphere electrons escaping to the magnetosheath.

In this chapter, we present mantle plasma and HEEs in the midtail observed by ARTEMIS and the statistical dawn-dusk asymmetries in their occurrence. The results presented here are from an investigation extended from our previous studies [*Wang et al.*, 2014a, 2014b, and 2015] with a larger data set included. We describe ARTEMIS measurements and data selections in section 17.2. In section 17.3, we describe the occurrence and characteristics of mantle plasma and discuss the solar-wind–magnetosphere processes responsible for dawn-dusk asymmetry by comparing the observations with predictions from global MHD simulations. In section 17.4, we present the characteristics and the dawn-dusk asymmetry of HEEs and, from their correlations with the solar-wind/IMF conditions, discuss the processes that likely lead to this asymmetry.

17.2. DATA

The two identically instrumented ARTEMIS probes (P1 and P2) [*Sibeck et al.*, 2011] are in lunar orbit (r ~60 R_E) and remain close to the Moon with distances < ~5 R_E from the Moon. ARTEMIS data have been available since August 2010. It takes roughly 2 days for each probe to laterally cross the dusk side or dawn side magnetosheath and ~4–5 days to cross the tail magnetosphere. Particle and magnetic field measurements with 1 min resolution are used. Ions and electrons are measured by an electrostatic analyzer (ESA, 0.006–20 keV/q [*McFadden et al.*, 2008]). The magnetic field is measured by the flux gate magnetometer [*Auster et al.*, 2008]. One minute solar wind and IMF parameters obtained from NASA OMNI and shifted to the X locations of the ARTEMIS probes are used.

We used 5 years of ARTEMIS data from August 2010 to August 2015 and selected mantle plasma and HEEs employing the same selection criteria as in *Wang et al.* [2014a, 2015]. To select mantle plasma, we first visually examined the plasma density and parallel velocity, magnetic field, and energy spectra to identify periods of mantle plasma, and we then further excluded ambiguous data points by selecting data within identified periods with the criteria: $N \geq 0.08\,\mathrm{cm}^{-3}$, $N/N_{SW} \leq 1$, $T \leq 0.5$ keV, $|B_x| \geq 5$ nT, and $V_{\parallel, x} \leq -30$ km/s. Since most of our mantle plasma has Bz/Br ($Br = \sqrt{Bx2 + By2}$) less than 0.6 and plasma beta less than 1, we used $Bz/Br \leq 0.6$ and plasma beta < 1 to identify the ARTEMIS probes being in the lobe region when they were inside the magnetosphere. The mantle and lobe are above (below) the current sheet if B_x is positive (negative). Data within 10 Moon radii were also excluded to avoid Moon pickup ions.

The following procedures were used to select HEEs: (1) We first selected magnetosheath data on the nightside using criteria: $X < 0$ and $|Y| \leq 60$ R_E, electron temperature (T_e) ≤ 70 eV, energy flux for 9 keV electrons ≤ $2 \cdot 10^4$ eV/s-sr-cm^2-eV, and bulk speed (V_x) and density (N) satisfy either ($V_x \leq -200$ km/s and $N \geq 2\,\mathrm{cm}^{-3}$) or ($V_x \leq -300$ km/s and $N \geq 0.9\,\mathrm{cm}^{-3}$). (2) From these magnetosheath data, we computed hourly median values of the energy fluxes for 1, 4, and 9 keV electrons to be used as the background fluxes. (3) A data point was selected as an enhancement if its 1 keV electron flux was a factor of 3 larger and its 4 and 9 keV fluxes were larger than the background fluxes, and its location was outside the main magnetopause and $|dY| \leq 20$ R_E, where $dY = Y_{probe} - Y_{magnetopause}$, and inside the main bow shock and at least 2 R_E away from the bow

shock (see *Wang et al.* [2015] for detailed procedures of determining the main magnetopause and bow shock from each ARTEMIS pass). As can be seen in the example shown in Figure 17.1a, in the midtail, mantle plasma can be observed deep inside the magnetosphere and HEEs can be observed at different Y distances from the magnetopause.

17.3. MANTLE PLASMA

17.3.1. Dawn-Dusk Asymmetry and Characteristics

Figure 17.2 shows the number of data points for the lobe and mantle on the top and the occurrence rates of mantle plasma on the bottom. The mantle plasma can be observed throughout the magnetotail with occurrence rates about 50% near the flanks but decreasing quickly with decreasing $|Y|$ to nearly 0% at midnight. The mantle occurrence rates at different locations are found to depend strongly on the IMF B_y direction, but not on IMF B_x or IMF B_z. Figure 17.2 shows that in the region above the current sheet ($B_x > 0$), mantle plasma appears dominantly in the postmidnight (premidnight) sector when the IMF B_y is positive (negative). The asymmetry is opposite in the region below the current sheet. These asymmetries are consistent with those obtained by *Wang et al.* [2014a] from a smaller dataset.

Figure 17.3a shows the correlations of normalized density (normalized to the solar-wind density) and $|V_\perp|$ with $|V_\parallel|$ under a specific range of solar-wind/IMF conditions ($3 \le N_{SW} \le 4\,cm^{-3}$, $450 \le V_{SW} \le 550$ km/s, and |IMF B_z | ≤ 1 nT). The mantle density is found to be highly correlated with $|V_\parallel|$, consistent with the 1-D MHD prediction [*Siscoe and Sanchez*, 1987; *Siscoe et al.*, 1994]. Most data points in the N-$V_\parallel$ plot fall between a lower and an upper limit lines indicated by the black lines, which are a linear function of the $V_\parallel$ speed ($\log_{10}[N] = \log_{10}[N_0] + C \cdot |V_\parallel|$, where N_0 is the density limit. The constants N_0 and C are different for the two lines, and their values also change with different ranges of solar-wind/IMF B_z conditions). $|V_\perp|$ is generally larger when $|V_\parallel|$ is larger, but the correlation is not as strong as the N-$V_\parallel$ correlation. Figure 17.3b shows the Y-profiles of normalized density and $V_\parallel$ for |IMF B_z | < 1 nT. The normalized density decreases by a factor of ~5 decreasing $|Y|$ while $V_\parallel$ decreases by a factor of ~2.5. These Y-profiles are consistent with the predicted profiles of *Pilipp and Morfill* [1978] when assuming that the sources for mantle plasma are particles entering through the magnetotail magnetopause along open field lines (open magnetopause) and that this magnetopause source extends continuously down the magnetotail.

17.3.2. Comparisons with Global MHD Simulations

To check whether the observed dawn-dusk asymmetry shown in Figure 17.2 and characteristics shown in Figure 17.3a and b can be reproduced by global MHD models, we examined the results from a BATS-R-US 3D global MHD simulation [*Powell et al.*, 1999; *Tóth et al.*, 2012] that is available from the simulations that have been conducted at the Community Coordinated Modeling Center (CCMC) at NASA Goddard Space Flight Center. This simulation was run with a 0° dipole tilt angle under steady upstream solar wind and IMF conditions: IMF $B_y = 7.15$ nT, IMF $B_z = 0$, $V_{SW} = V_{SW,\,x} = -560$ km/s, $N_{SW} = 3.3\,cm^{-3}$, and $T_{SW} = 116{,}040$ K. The simulation run was used in *Sibeck and Lin* [2014] to investigate the size and shape of the midtail magnetosphere.

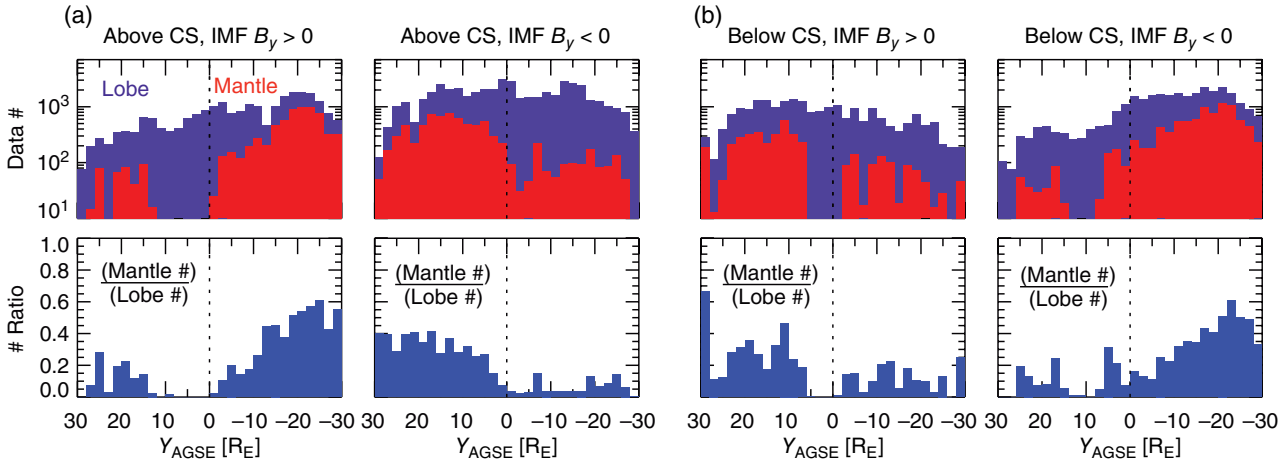

Figure 17.2 The number of data points in the lobe region (dark gray) and the mantle (light gray) (top) and the ratios of the number of the mantle data points to that in the lobe region (bottom) under positive or negative IMF B_y (a) above and (b) below the current sheet.

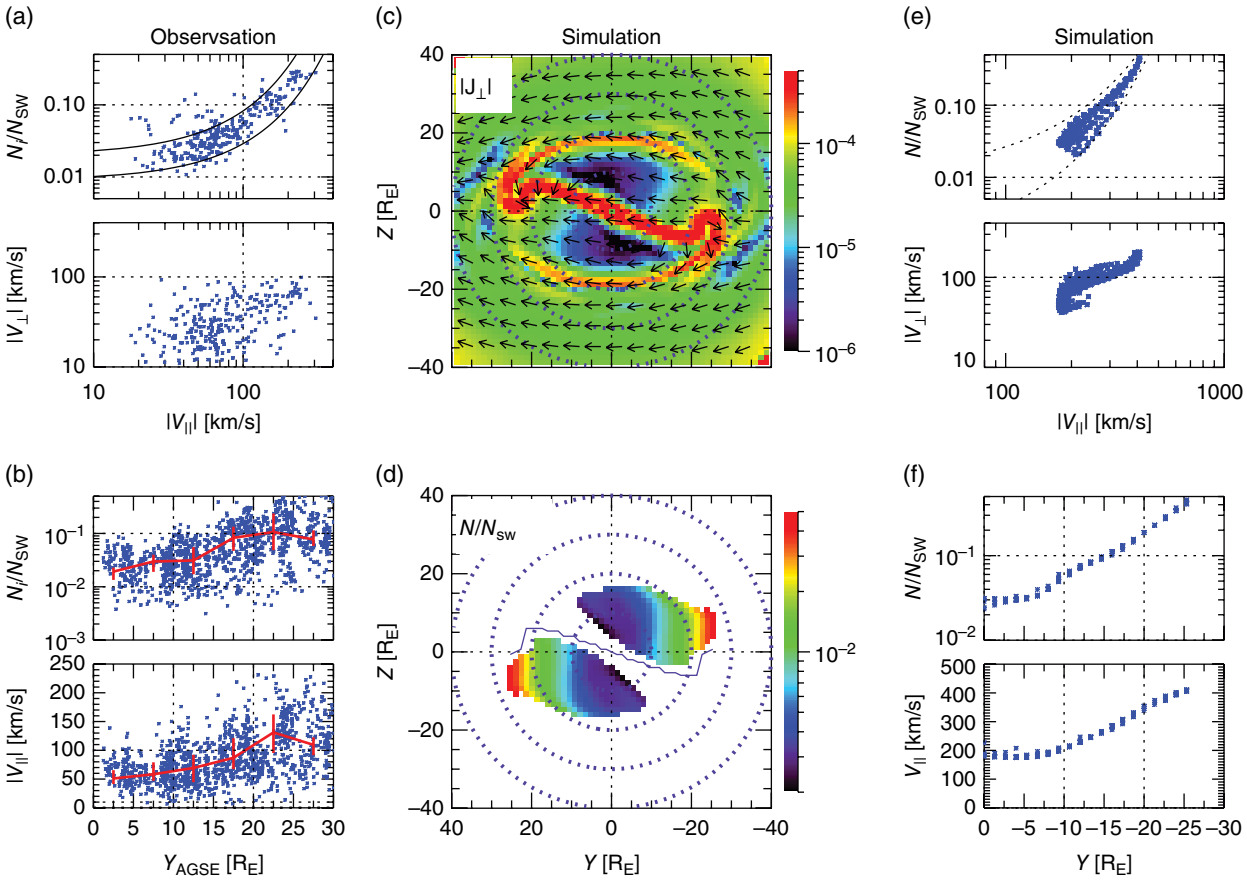

Figure 17.3 Comparisons of ARTEMIS observations with MHD simulations. (a) N/N_{SW} and $|V_\perp|$ as a function of $|V_{||}|$ and (b) N/N_{SW} and $|V_{||}|$ as a function of Y for the observed mantle plasma (the solid gray indicate median values and the 25% and 75% quartiles). The Y-Z distributions of (c) $|J_\perp|$ and (d) mantle density normalized to the solar-wind density at $X = -60$ R_E from the simulation. (e) N/N_{SW} and $|V_\perp|$ as a function of $|V_{||}|$ and (f) N/N_{SW} and $|V_{||}|$ as a function of Y for the simulated mantle plasma.

Figure 17.3c shows Y-Z profiles of the simulated perpendicular current density ($|J_\perp|$) at $X = -60$ R_E. The locations of the magnetopause and current sheet can be identified by their relatively large current density. The spatial distributions of the normalized density for mantle plasma are shown in Figure 17.3d. The appearance of mantle plasma in the region above or below the current sheet has a clear dawn-dusk asymmetry. Positive IMF B_y is specified for this simulation and mantle plasma above the current sheet appears on the dawn side, consistent with the observed asymmetry shown in Figure 17.2. Correlations of normalized density and $V_\perp$ speed with $V_{||}$ for simulated mantle plasma are shown in Figure 17.3e. The simulated correlations are qualitatively consistent with the observed correlations shown in Figure 17.3a, with the simulated densities also falling between a lower and an upper limit lines, as indicated by the black dotted lines, with logarithm of the density limit being a linear function of $|V_{||}|$. Figure 17.3f shows that both simulated mantle plasma density and $V_\perp$ speed decrease with decreasing $|Y|$, in good agreement with the observed Y-profiles shown in Figure 17.3b.

Figure 17.3c, d shows that the simulated mantle density is highest just inside the magnetopause at the location where the magnetopause current density is weakest. This location is where magnetosheath plasma gets access to the magnetosphere and also where magnetic field lines are open, as indicated by the black arrows for magnetic field directions shown in Figure 17.3c. We also examined other BATS-R-US simulations under the same solar-wind/IMF conditions but with different |IMF B_y|/|IMF B_z| ratios. These simulations show that when IMF B_y becomes more dominant, the locations of open magnetopause and the resulting mantle plasma move to lower latitudes and to opposite sides of the magnetosphere above and below the current sheet. Therefore, the observed dawn-dusk asymmetry in the midtail mantle plasma is a result of the IMF B_y dependence of the processes that create an open magnetopause.

17.4. HOT ELECTRON ENHANCEMENTS

17.4.1. Characteristics

The duration for the majority of HEEs is fewer than ~2 min, and they are separated from each other by a few minutes. In our previous study using simultaneous measurements from the two ARTEMIS probes to determine the source and spatial structures of HEEs [*Wang et al.*, 2014], we found the following: (1) The source for the hot electrons in HEEs is the magnetosphere electrons. (2) HEEs are associated with bursty lateral magnetosphere intrusion into the magnetosheath, that is, magnetopause outward deformation. (3) Using observations when the two probes are aligned mainly along the *X* or *Y* direction to estimate the *X* and *Y* scales of a HEE, a single HEE can have an elongated structure as narrow as 2 R_E wide in the *X* direction and in some cases as long as over 7 R_E in the *Y* direction. (4) HEEs move tailward with speeds similar to those of background magnetosheath flows. The results suggest that HEEs are a result of two solar-wind–magnetosphere coupling processes: (1) transient and localized magnetopause deformation caused by processes such as Kelvin-Helmholtz (K-H) waves or magnetosheath density perturbations, and (2) subsequent secondary processes, such as reconnection or diffusion, along the deformed magnetopause that allow the magnetosphere electrons to enter the magnetosheath. Illustration of a HEE based on the above conclusion is shown in Figure 5 of *Wang et al.* [2014]. The elongated HEE structure along the *Y* direction might also be formed by hot magnetosphere electrons entering the magnetosheath through magnetic drift and then streaming away from the magnetopause along *By*-dominant magnetosheath magnetic fields, however, observations of HEEs show that such *By*-dominant fields do not often exist.

17.4.2. Dawn-Dusk Asymmetry

Figure 17.4a shows the number of 1 min data points for magnetosheath data (dark gray) and for HEEs (light gray), and Figure 17.4b shows the HEE occurrence rate as a function of *dY*, where *dY* is positive (negative) for the dusk side (dawn side). The number of magnetosheath data points is relatively constant across the magnetosheath and has no clear dawn-dusk asymmetry. There is a clear dawn-dusk asymmetry in the HEE numbers with 3259 HEEs on the dawn side and 1224 on the dusk side. So the HEE occurrence rates are a factor of 2 to 3 higher on the dawn side than on the dusk side. This factor is slightly lower than that obtained by *Wang et al.* [2015] from a smaller dataset.

To investigate likely causes of this dawn-dusk asymmetry, we examine whether HEEs occur more often under certain solar-wind/IMF conditions in comparison to typical magnetosheath plasma. Since a HEE only lasts for ~2 min but the uncertainty in the OMNI solar-wind/IMF is much larger due to the estimated time shift, here we use the magnetosheath plasma and magnetic field to represent the solar-wind/IMF conditions since they reflect concurrent solar-wind/IMF conditions more precisely in time than do the OMNI solar-wind/IMF data. Figure 17.5 shows the probability distributions for the plasma and magnetic field parameters in the magnetosheath corresponding to HEE data points (in light gray) in comparison with those corresponding to all magnetosheath data points (in dark gray) on the dawn side and dusk side. Compared with typical magnetosheath plasma, it is clear that HEEs occur during periods of relatively lower solar-wind–magnetosheath density and higher solar-wind–magnetosheath speed (since the solar-wind density is well anticorrelated with the solar-wind speed). In addition, they are accompanied by larger transient density changes in the magnetosheath, indicated by a parameter $dN/N = (N_{max} - N_{min})/N_{ave}$, where N_{max}, N_{min}, and N_{ave} are the maximum, minimum, and average values of densities within the ±5 min period of a data point. These correlations with higher solar-wind speed and larger magnetosheath density changes are stronger on the dawn side than on the dusk side. Furthermore, HEEs occur more often when the magnitude of B_z is smaller and are more often associated with sharp B_z changes, as indicated by a parameter $dB_z = (|B_{z,\,max}| - |B_{z,\,min}|)/[\mathrm{sign}(B_{z,\,max}) \cdot \mathrm{sign}(B_{z,\,min})]$, where $B_{z,\,max}$ ($B_{z,\,min}$) and sign($B_{z,\,max}$) (sign($B_{z,\,min}$)) are the magnitude and sign of the maximum (the minimum) B_z. If the B_z change within the 10 min is sharper, then $|dB_z|$ is larger, and dB_z is negative if there is a B_z direction change.

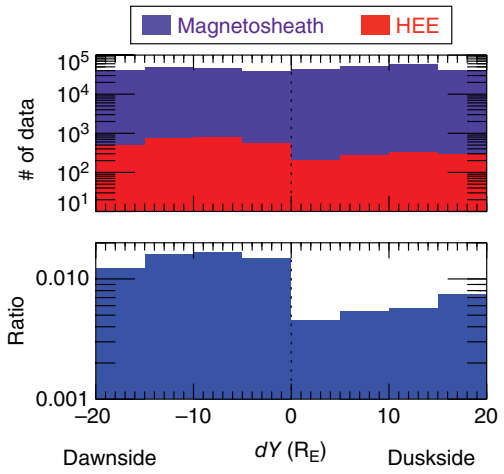

Figure 17.4 Number of 1 min data points for the magnetosheath (dark gray) and HEEs (light gray) (top) and the ratios of the number of HEEs to that of the magnetosheath data (bottom) as a function of *dY*, the *Y* distance to the magnetopause. Positive (negative) *dY* indicates the dusk side (dawn side).

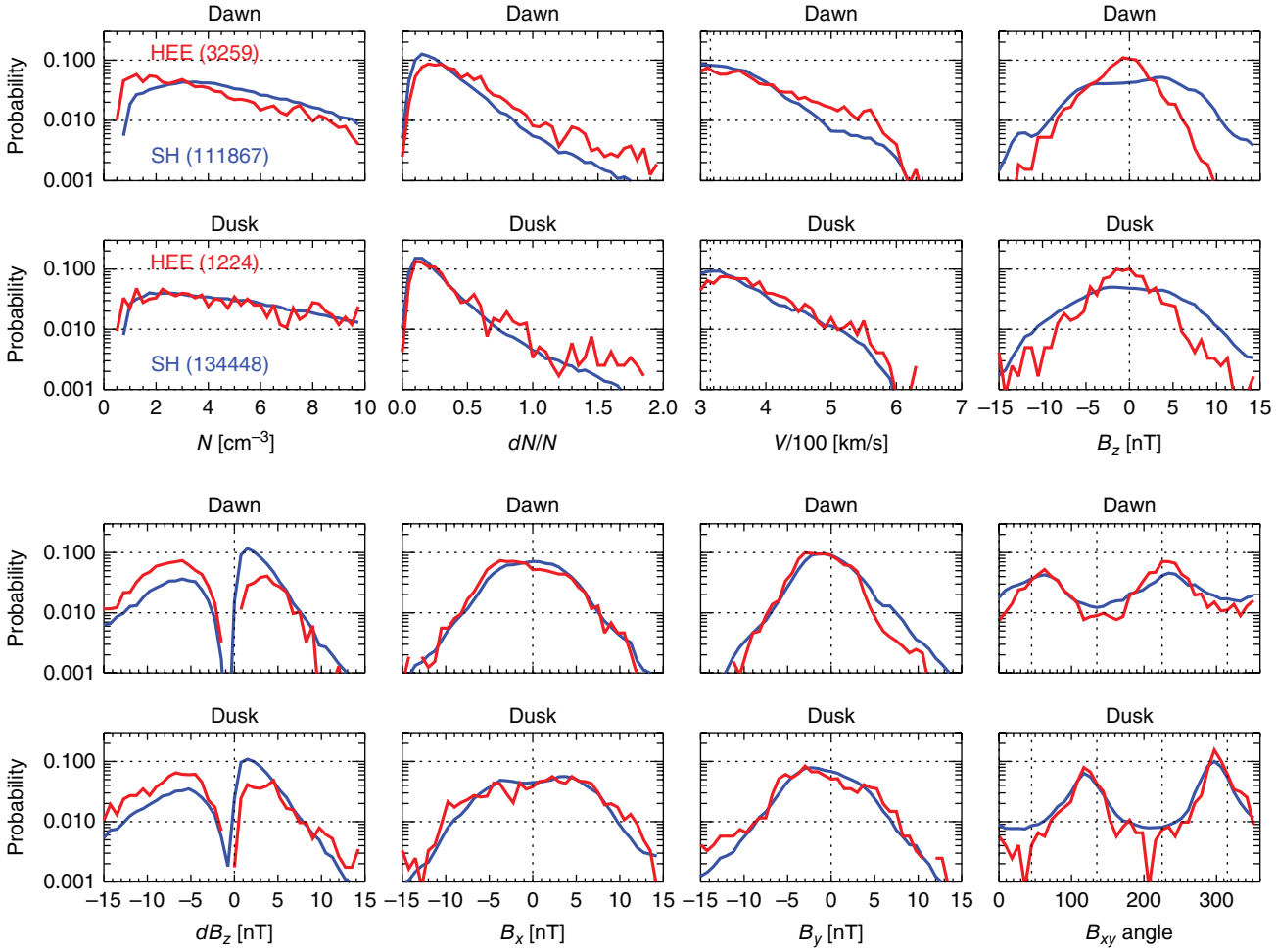

Figure 17.5 Probability distributions of density, dN/N, flow speed, B_z, dB_z, B_x, B_y, and B_{xy} angle (see text for definitions of dN/N, dB_z and B_{xy} angle) observed by ARTEMIS for the magnetosheath (dark gray) and HEEs data (light gray) on the dawnside and duskside. The numbers inside the parenthesis indicate the number of data points for each data set.

There are no clear differences between HEEs and magnetosheath plasma on their B_x and B_y probability distributions, but there are noticeable differences in the distributions of the B_{xy} angles. The B_{xy} angle probability distributions for all magnetosheath data peak at ~45° and 225° on the dawn side and at ~135° and 315° on the dusk side, indicating that the corresponding IMF is a Parker spiral (~135° or 315°) most of the time. The B_{xy} angles are rotated about 90° from the Parker-spiral angles on the dawn side magnetosheath but are similar to the Parker-spiral angles on the dusk side magnetosheath because the magnetosheath magnetic field lines on the side where the bow shock is quasiparallel (quasiperpendicular) are refracted away from the shock normal (are draped over [tangential to] the magnetopause). In comparison, on the dawn side, the B_{xy} angle probabilities for HEEs become higher at ~45° and 225°, but on the dusk side the probabilities for HEEs at ~45° and 225° become significantly lower. The differences indicate that dawn-side HEEs occur preferentially when the quasiparallel bow shock is on the dawn side and some, but not the majority, of the dusk-side HEEs occur when the quasiparallel bow shock is on the dusk side, that is, anti-Parker-spiral IMF (~45° or 225°).

The above preferred conditions for HEEs in transient magnetosheath density changes, transient B_z changes, and the B_{xy} angles suggest a possible connection between the perturbations created at the quasiparallel bow shock and HEEs. Many bow-shock processes associated with changing IMF (IMF discontinuities) are known to create transient and mesoscale (in a timescale of a few minutes and a spatial scale of a few to 10 R_E), but substantial, density and dynamic pressure perturbations in the magnetosheath, such as hot flow anomalies (HFAs) [e.g., *Thomsen et al.*, 1986; *Schwartz*, 1995; *Zhang et al.*, 2010], foreshock bubbles (FBs) [e.g., *Omidi et al.*, 2010; *Turner et al.*, 2013], magnetosheath filamentary structures (MFSs) [*Omidi et al.*, 2014], and transient flux enhancements or

jets [e.g., *Němeček et al.*, 1998, *Hietala et al.*, 2012]. Observations from multiple spacecraft have shown that the resulting density perturbations in the magnetosheath can cause localized deformation of the dayside magnetopause [e.g., *Hietala et al.*, 2012; *Archer et al.*, 2015]. It has been suggested that as bow-shock perturbations move tailward, they can continue to cause magnetopause deformation farther down the tail [*Sibeck et al.*, 1999]. HFA-like events have been observed by ARTEMIS in the midtail magnetosheath [*Wang et al.*, 2015] and by STEREO at 310 R_E in the tail magnetosheath [*Facskó et al.*, 2015]. Thus the magnetopause deformation resulting from the bow-shock perturbations can possibly lead to HEEs in the midtail. Since many bow-shock perturbations are generated in the quasiparallel bow shock, which is mostly on the dawn side due to the Parker-spiral IMF, the connection of HEEs with quasiparallel bow-shock perturbations may explain the higher HEE occurrence rates on the dawn side. This mechanism could be further investigated in the future by using global hybrid simulations with the midtail magnetosheath and magnetosphere included. The detailed mechanism of how the solar-wind–magnetosphere associated with the locally deformed magnetopause can lead to HEEs can be investigated with 3D full particle (ions and electrons) simulations using particle-in-cell codes [e.g., *Nakamura et al.*, 2013] in the future. Although HEEs can also be associated with K-H perturbations, our current understanding of the dawn-dusk asymmetry in the occurrence of the K-H perturbations, especially in the midtail, is insufficient to determine their contribution to HEE asymmetry.

17.5. SUMMARY

Both mantle plasma and HEEs result from plasma transfer across the magnetopause. We analyzed the occurrence of these two populations in the midtail using 5 years of ARTEMIS observations to determine their dawn-dusk asymmetries and the likely responsible solar-wind–magnetosphere coupling processes. Our main conclusions are as follows:

1. There is a strong dawn-dusk asymmetry in the appearance of mantle plasma depending on the IMF B_y direction, with higher occurrence rates in the postmidnight (premidnight) sector above the current sheet when the IMF B_y is positive (negative). Opposite dawn-dusk asymmetries are seen below the current sheet.

2. The main characteristics of mantle plasma and their crosstail profiles and the observed dawn-dusk asymmetry are qualitatively consistent with predictions from BATS-R-US global MHD simulations. These simulations indicate that mantle plasma in the midtail results from magnetosheath plasma crossing the tail magnetopause along the open field lines, and that the dawn-dusk asymmetry is a result of the open magnetopause region moving to lower latitudes and to opposite sides of the magnetosphere above and below the current sheet when the IMF B_y becomes more dominant.

3. HEEs are associated with solar-wind–magnetosphere coupling processes that cause transient and localized magnetopause deformation and subsequent secondary processes that cause the magnetosphere electrons next to the deformed magnetopause to enter the magnetosheath.

4. HEE occurrence rates on the dawn side are about a factor of 2 to 3 higher than those on the dusk side. Compared with typical magnetosheath plasma, the majority of HEEs are associated with higher solar-wind speed, larger transient density changes in the magnetosheath, sharper transient IMF direction changes, and quasiparallel bow shock. These correlations suggest a connection between HEEs and the magnetopause deformation caused by density perturbations created at the quasiparallel shock, such as HFAs and FBs. Since the quasiparallel shock is most often on the dawn side, this connection is likely to cause higher HEE occurrence rates on the dawn side.

ACKNOWLEDGMENTS

The work by C.-P. Wang and L. R. Lyons has been supported by NASA Grant NNX11AJ12G and NSF Grant ATM-1003595. The work by X. Xing has been supported by NASA grant NNX12AD11G. We acknowledge NASA contract NAS5-02099 for ARTEMIS; C. W. Carlson and J. P. McFadden for the use of ESA data; D. Larson and R. P. Lin for use of the SST data; and K. H. Glassmeier, U. Auster, and W. Baumjohann for the use of FGM data provided under DLR contract 50 OC 0302. The ARTEMIS data are available online (http://artemis.ssl.berkeley.edu/) for free. Simulation results have been provided by the Community Coordinated Modeling Center (CCMC) free of charge at Goddard Space Flight Center through its public Runs on Request system (http://ccmc.gsfc.nasa.gov). In particular, we have studied the run "Claire_Kuang_071X11_X". The BATS-R-US Model was developed by the CSEM group at the University of Michigan. We thank T. Gombosi at the University of Michigan for helpful discussion of the simulation results. We thank J. H. King, N. Papatashvilli at AdnetSystems, NASA GSFC and CDAWeb for providing the OMNI data. We thank Hui Zhang at the University of Alaska, Drew Turner at Aerospace Corporation, and A. Poppe at the University of California at Berkeley for their helpful discussion.

REFERENCES

Archer, M. O., D. L. Tuner, J. P. Eastwood, S. J. Schwartz, and T. S. Horbury (2015), Global impacts of a foreshock bubble: Magnetosheath, magnetopause, and ground-based observations, *Planet. Space Sci.*, *106*; doi:10.1016/j.pss.2014.11.026.

Auster, H. U., *et al.* (2008), The THEMIS fluxgate magnetometer, *Space Sci. Rev.*, *141*, 235–264; doi:10.1007/s11214-008-9365-9.

Facskó, G., A. Opitz, B. Lavraud, J. G. Luhmann, C. T. Russell, J.-A. Sauvaud, A. Fedorov, A. Kis, and V. Wesztergom (2015), Hot flow anomaly remnant in the far geotail? *J. Atmos. Solar Terr. Phys.*, *124*, 39–43.

Gosling, J. T., D. N. Baker, S. J. Bame, E. W. Hones Jr., D. J. McComas, R. D. Zwickl, J. A. Slavin, E. J. Smith, and B. T. Tsurutani (1984), Plasma entry into the distant tail lobes: ISEE-3, *Geophys. Res. Lett.*, *11*(10), 1078–1081; doi:10.1029/GL011i010p01078.

Haerendel, G., and G. Paschmann (1975), Entry of solar wind plasma into the magnetosphere, *Physics of the Hot Plasma in the Magnetosphere*, edited by B. Hultqvist and L. Stenflo, 23–43, Plenum, New York.

Hardy, D. A., H. K. Hills, and J. W. Freeman (1975), A new plasma regime in the distant geomagnetic tail, *Geophys. Res. Lett.*, *2*, 169–172; doi: 10.1029/GL002i005p00169.

Hardy, D. A., H. K. Hills, and J. W. Freeman (1979), Occurrence of the lobe plasma at lunar distance, *J. Geophys. Res.*, *84*(A1), 72–78; doi:10.1029/JA084iA01p00072.

Hardy, D. A., J. W. Freeman, and H. K. Hills (1976), Plasma observations in the magnetotail, in *Magnetospheric Particles and Fields*, edited by B. M. McCormac, *89*, D. Reidel, Hingham, MA.

Hietala, H., N. Partamies, T.-V. Laitinen, L.-B. N. Clausen, G. Facskó, A. Vaivads, H. E. J. Koskinen, I. Dandouras, H. Rème, and E. A. Lucek (2012), Supermagnetosonic subsolar magnetosheath jets and their effects: From the solar wind to the ionospheric convection, *Ann. Geophys.*, *30*, 33–48; doi:10.5194/angeo-30-33-2012.

Imada, S., M. Hoshino, and T. Mukai (2005), The dawn-dusk asymmetry in magnetosheath and the leakage of energetic electrons: The Geotail observation, in *Frontiers in Magnetospheric Plasma Physics: Celebrating 10 Years of Geotail Operation*, Cospar Colloquia Series, *16*, edited by M. Hoshino *et al.*, 34–39, Elsevier, New York.

Maezawa, K. and T. Hori (1998), The distant magnetotail: Its structure, IMF dependence, and thermal properties, in *New Perspectives on the Earth's Magnetotail*, edited by Nishida *et al.*, 1–20, Geophysical Monograph Series, *105*, American Geophysical Union, Washington, DC.

McFadden, J. P., C. W. Carlson, D. Larson, V. Angelopoulos, M. Ludlam, R. Abiad, B. Elliott, P. Turin, and M. Marckwordt (2008), The THEMIS ESA plasma instrument and inflight calibration, *Space Sci. Rev.*, *141*, 277–302; doi:10.1007/s11214-008-9440-2.

Nakamura, T. K. M., W. Daughton, H. Karimabadi, and S. Eriksson (2013), Three-dimensional dynamics of vortex-induced reconnection and comparison with THEMIS observations, *J. Geophys. Res. Space Physics*, *118*, 5742–5757; doi:10.1002/jgra.50547.

Němeček, Z., J. Šafránková, L. Prech, D. G. Sibeck, S. Kokubun, and T. Mukai (1998), Transient flux enhancements in the magnetosheath, *Geophys. Res. Lett.*, *25*, 1273–1276; doi:10.1029/98GL50873.

Omidi, N., D. Sibeck, O. Gutynska, and K. J. Trattner (2014), Magnetosheath filamentary structures formed by ion acceleration at the quasi-parallel bow shock, *J. Geophys. Res. Space Physics*, *119*, 2593–2604; doi:10.1002/2013JA019587.

Omidi, N., J. P. Eastwood, and D. G. Sibeck (2010), Foreshock bubbles and their global magnetospheric impacts, *J. Geophys. Res.*, *115*, A06204.

Pilipp, W. G., and G. Morfill (1978), The formation of the plasma sheet resulting from plasma mantle dynamics, *J. Geophys. Res.*, *83*(A12), 5670–5678; doi:10.1029/JA083iA12p05670.

Powell, K. G., P. L. Roe, T. J. Linde, T. I. Gombosi, and D. L. de Zeeuw (1999), A solution-adaptive upwind scheme for ideal magnetohydrodynamics, *J. Comput. Phys.*, *154*, 284–309; doi:10.1006/jcph.1999.6299.

Sarafopoulos, D. V., M. A. Athanasiu, D. G. Sibeck, R. W. McEntire, E. T. Sarris, and S. Kokubun (2000), Energetic proton and electron dispersion signatures in the nightside magnetosheath support their leakage out of the magnetopause, *J. Geophys. Res.*, *105*, 15,729–15,740.

Scholer, M., F. M. Ipavich, G. Gloeckler, D. Hovestadt, and B. Klecker (1981), Leakage of magnetospheric ions into the magnetosheath along reconnected field lines at the dayside magnetopause, *J. Geophys. Res.*, *86*(A3), 1299–1304; doi:10.1029/JA086iA03p01299.

Seki, K., M. Hirahara, T. Terasawa, T. Mukai, and S. Kokubun (2000), Origin and dynamics of multicomponent (H+/He++/He+/O+) ion flows in the lobe/ mantle regions, *Adv. Space Res.*, *25*(7–8), 1581–1590.

Seki, K., M. Hirahara, T. Terasawa, T. Mukai, Y. Saito, S. Machida, T. Yamamoto, and S. Kokubun (1998), Statistical properties and possible supply mechanisms of tailward cold O^+ beams in the lobe/mantle regions, *J. Geophys. Res.*, *103*(A3), 4477–4489; doi:10.1029/97JA02137.

Schwartz, S. J. (1995), Hot flow anomalies near the Earth's bow shock, *Adv. Space Res.*, *15*, 107–116; doi:10.1016/0273-1177(95)00025-A.

Sibeck, D. G., R. W. McEntire, A. T. Y. Lui, R. E. Lopez, S. M. Krimigis, R. B. Decker, L. J. Zanetti, and T. A. Potemra (1987), Energetic magnetospheric ions at the magnetopause: Leakage or merging?, *J. Geophys. Res.*, *92*, 12,097–12,114.

Sibeck, D. G., *et al.* (1999), Comprehensive study of the magnetospheric response to a hot flow anomaly, *J. Geophys. Res.*, *104*(A3), 4577–4593; doi:10.1029/1998JA900021.

Sibeck, D. G., *et al.* (2011), ARTEMIS science objectives, *Space Sci Rev.*, *165*, 59–91; doi 10.1007/s11214-011-9777-9.

Sibeck, D. G., and R.-Q. Lin (2014), Size and shape of the distant magnetotail, *J. Geophys. Res. Space Physics*, *119*; doi:10.1002/2013JA019471.

Siscoe, G. L., and E. Sanchez (1987), An MHD model for the complete open magnetotail boundary, *J. Geophys. Res.*, *92*(A7), 7405–7412; doi:10.1029/JA092iA07p07405.

Siscoe, G. L., L. A. Frank, K. L. Ackerson, and W. R. Paterson (1994), Properties of mantle-like magnetotail boundary layer: Geotail data compared with a mantle model, *Geophys. Res. Lett.*, *21*, 2975–2978.

Siscoe, G. L., G. M. Erickson, B. U. Sonnerup, N. C. Maynard, K. D. Siebert, D. R. Weimer, and W. W. White (2001), Relation between cusp and mantle in MHD simulation, *J. Geophys. Res.*, *106*(A6), 10743–10749; doi:10.1029/2000JA000385.

Taguchi, S., H. Kishida, T. Mukai, and Y. Saito (2001), Low-latitude plasma mantle in the near-Earth magnetosphere: Geotail observations, *J. Geophys. Res. Space Physics* (1978–2012), *106*, A2.

Thomsen, M. F., J. T. Gosling, S. A. Fuselier, S. J. Bame, and C. T. Russell (1986), Hot, diamagnetic cavities upstream from the Earth's bow shock, *J. Geophys. Res.*, *91*, 2961–2973; doi:10.1029/JA091iA03p02961.

Tóth, G., *et al.* (2012), Adaptive numerical algorithms in space weather modeling, *J. Comput. Phys.*, *231*, 870–903; doi:10.1016/j.jcp.2011.02.006.

Turner, D. L., N. Omidi, D. G. Sibeck, and V. Angelopoulos (2013), First observations of foreshock bubbles upstream of Earth's bow shock: Characteristics and comparisons to HFAs, *J. Geophys. Res. Space Physics*, *118*, 1552–1570; doi:10.1002/jgra.50198.

Wang, C.-P., L. R. Lyons, and V. Angelopoulos (2014a), Properties of low-latitude mantle plasma in the Earth's magnetotail: ARTEMIS observations and global MHD predictions, *J. Geophys. Res. Space Physics*, *119*, 7264–7280; doi:10.1002/2014JA020060.

Wang, C.-P., X. Xing, T. K. M. Nakamura, and L. R. Lyons (2015), Dawn-dusk asymmetry in bursty hot electron enhancements in the mid-tail magnetosheath, *J. Geophys. Res. Space Physics*, *120*; doi:10.1002/2015JA021522.

Wang, C.-P., X. Xing, T. K. M. Nakamura, L. R. Lyons, and V. Angelopoulos (2014b), Source and structure of bursty hot electron enhancements in the tail magnetosheath: Simultaneous two-probe observation by ARTEMIS, *J. Geophys. Res. Space Physics*, *119*, 9900–9918; doi:10.1002/2014JA020603.

Zhang, H., D. G. Sibeck, Q.-G. Zong, S. P. Gary, J. P. McFadden, D. Larson, K.-H. Glassmeier, and V. Angelopoulos (2010), Time history of events and macroscale interactions during substorms observations of a series of hot flow anomaly events, *J. Geophys. Res.*, *115*, A12235; doi:10.1029/2009JA015180.